ELSEVIER

Journal of Structural Geology 27 (2005) 1205–1216

JOURNAL OF STRUCTURAL GEOLOGY

www.elsevier.com/locate/jsg

Distribution of non-plane strain in experimental compression of short cylinders of Solnhofen limestone

Sergio Llana-Fúnez*, Ernest H. Rutter

School of Earth, Atmospheric and Environmental Sciences, University of Manchester, Oxford Road, Manchester M13 9PL, UK

Received 2 April 2003; received in revised form 4 February 2004; accepted 19 August 2004
Available online 9 June 2005

Abstract

Axi-symmetric compression experiments on short cylinders (radius > length) have great potential for the investigation of different non-plane strain geometries. In such experiments strain geometry and intensity are heterogeneously distributed throughout the specimens due to the effects of friction at the contact surface between the pistons and the specimen. We ran a series of tests on Solnhofen limestone at constant confining pressure (200 MPa), temperature (600 °C) and displacement rate (5.2×10^{-6} m s^{-1}), conditions at which this material deforms predominantly by crystal plasticity. Using shape and crystallographic preferred orientation (SPO and CPO) patterns of calcite grains, the latter measured by electron back-scattered diffraction techniques (EBSD), we can discriminate areas in the deformed specimens with distinct non-plane strain geometries. SPO and CPO patterns record differences in the orientation of the finite stretching direction with respect to the external reference frame. It is radial in the vicinities of the rigid loading pistons, but circumferential outside the periphery of the pistons. As shortening progressed, the middle part of the specimen was extruded with respect to the contacts with the rigid end pieces, imparting a non-coaxial component to the flow with a circumferential vorticity axis in both upper and lower halves of the specimen. This component was recorded in the microstructure as an asymmetric CPO. The aim of the experiments is to improve the interpretation of naturally deformed rock bodies when strain departs from plane strain conditions by using the CPO as a 3D kinematic indicator, providing not only shearing direction but also information about the shape in 3D of the strain ellipsoid.
© 2005 Elsevier Ltd. All rights reserved.

Keywords: Strain geometry; Solnhofen limestone; Experimental deformation; Microstructure; Electron back-scattered diffraction techniques (EBSD); Calcite

1. Introduction

A significant effort has been devoted in structural geology recently to the study of deformation in 3D, when deformation is non-planar. Several perspectives have been used for that purpose, from the strictly theoretical (e.g. Passchier, 1997, 1998), to numerical simulations (e.g. Jones et al., 1997) and even field observations (e.g. Passchier et al., 1997; Gilotti and Hull, 1993). In this context, this contribution makes some experimental observations from axi-symmetric compression of short cylinders because such experiments produce several non-plane strain geometries. Our experimental data may help in the understanding and interpretation of natural tectonic deformations where bulk and local non-plane strain components may be of significance.

There are a limited number of deformation geometries possible in standard rock deformation apparatus (Jaeger and Cook, 1976; Rutter, 1998). Traditionally, the aim has been to achieve a simple, constant and predictable flow geometry that matches homogeneously deformed rock bodies. One such example is the compression of long specimen cylinders. In this study, however, we did axi-symmetric compression on short cylinders of ultrafine-grained limestone ('short' referring to a length of the same order or magnitude as the radius of the cylinder), to a maximum bulk permanent shortening of 40–50%. The use of short cylinders increases the importance of friction effects at the contacts between the pistons and the specimen, causing heterogeneity of deformation, and allowing us to study a wide range of strain geometries and intensities within a single specimen (Fig. 1). These changes were recorded by variations in calcite crystallographic preferred orientation (CPO) patterns as well as the grain shape fabric.

* Corresponding author. Tel.: +44 161 2756913; fax: +44 161 2753947.
E-mail address: sergio.llana-funez@manchester.ac.uk (S. Llana-Fúnez).

0191-8141/$ - see front matter © 2005 Elsevier Ltd. All rights reserved.
doi:10.1016/j.jsg.2004.08.013

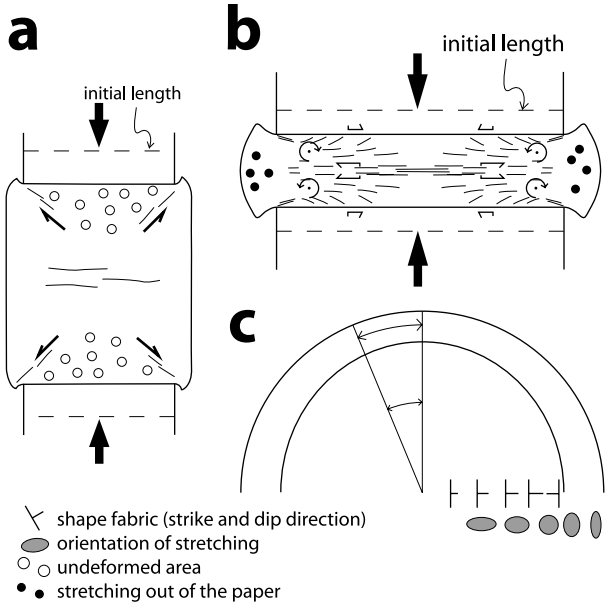

Fig. 1. Sketches showing the differences in shape fabric, strain intensity and their distribution in axi-symmetric compression of long (a) and short specimen cylinders (b). Note that to illustrate the curved nature of the shape fabric, dipping away from the specimen axis, strike and dip symbols are used in the map view in (b) (i.e. parallel to the specimen base). The length of the dip direction tick indicates the amount of dip: the lower the angles, the longer the ticks. Also, the orientation of the stretching direction is indicated by sketches of the relative orientation of the finite strain ellipse in this section.

One of the most significant results from our approach is that we were able to follow, using the microstructure, the effects of a 90° switch in the finite stretching direction. It is parallel to the cylinder radius in the vicinity of the pistons, but parallel to the circumference of the cylinder beyond the confines of the pistons. Thus, the orientation of the stretching direction with respect to the vorticity axis (which remains constantly circumferential) changes from being normal to stretch, as in general simple shear, to being parallel to it, as in the case of b-lineations (Sander, 1950) or X_i segments (Passchier, 1998). The effect of the non-coaxial component of the deformation shows up in the CPO patterns as external and internal asymmetries. Although our approach is so far empirical and qualitative, we consider it is a first step in the study of 3D deformation in mechanical experiments on rocks at elevated temperatures that may be comparable with some natural case-studies.

2. Experimental approach

2.1. Starting material

The starting material, Solnhofen limestone, has been widely used in experimental deformation studies and has several advantages for our purposes. The average grain size of Solnhofen limestone is 4–5 μm, with some larger grains dispersed throughout the rock (Fig. 2). This allows petrofabric studies to be made on a sufficiently large number of grains at several places within heterogeneously deformed specimens, despite the requirement to use a small diameter specimen (9.5 mm).

The initial porosity of the rock is approximately 5% (Rutter, 1972) and the rock comprises more than 97 wt% of calcite. Quartz grains of about 20 μm are present as a secondary phase (<0.1% volume) throughout the rock and some impurities, mostly organic matter and clay minerals, occur along grain boundaries (Schmid et al., 1977). These impurities act to impede grain growth (Walker et al., 1990; Rutter et al., 1994). The grain size and its rather uniform distribution, together with the low mobility of grain boundaries, make this material able to deform plastically at the conditions given below without interference from

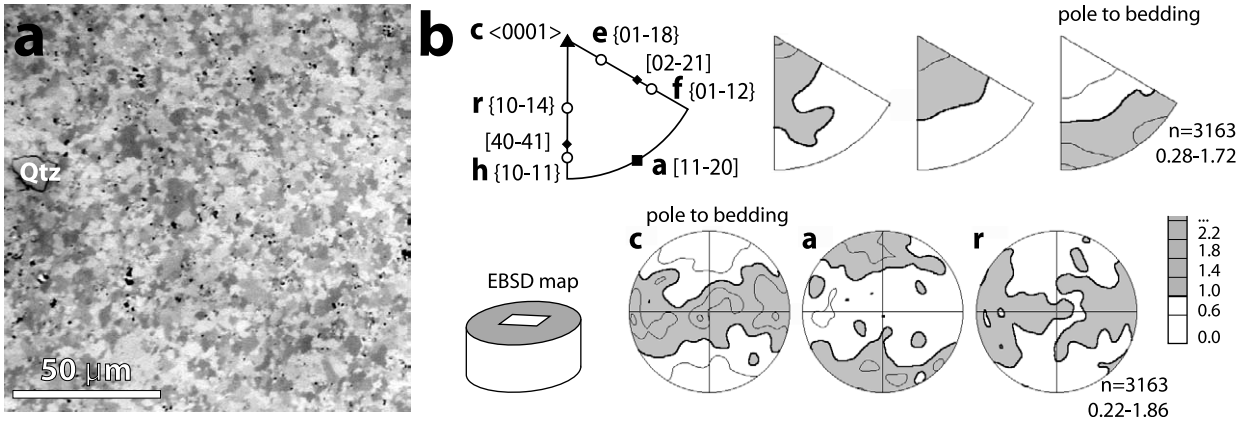

Fig. 2. Microstructure of the starting material for the experiments, Solnhofen limestone: (a) shows the microstructure in a micrograph taken with reflected light in a conventional optical microscope, and (b) shows the crystallographic preferred orientation (CPO) in calcite before the experiment. Contours in pole and inverse pole figures are every 0.4 multiples of uniform distribution (m.u.d.), starting at 0.6 m.u.d. Density areas above 1 m.u.d. are shaded. Inverse pole figures (top right in (b)) are presented with respect to the bedding plane and two perpendicular orientations selected at random but contained within the bedding plane. The upper left corner in (b) shows the significant crystallographic elements in the calcite lattice used in inverse pole figures. In IPF and pole figures *n* indicates the number of measurements and below this are the minimum and maximum intensities in m.u.d.

other processes that may alter grain shape or CPO (Schmid et al., 1977).

In previous experimental studies, combined measurement of CPO patterns and its relation with the shape fabric in Solnhofen limestone samples was not possible because the grain size was too small to measure the complete CPO with optical microscopy. Further, X-ray texture goniometry does not provide directly observable relationships with the shape fabric and requires homogeneous fabrics over a scale of several millimeters to obtain a CPO pattern. These limitations can now be overcome using electron backscattered diffraction (EBSD) techniques on polished surfaces of deformed specimens (see e.g. Prior et al., 1999).

Calcite in Solnhofen limestone has an initial CPO (Schmid et al., 1977; Rutter et al., 1994; Casey et al., 1998) characterized by a broad girdle of *c*-axes parallel to the bedding plane with a maximum intensity of 1.9 times uniform distribution (Fig. 2). This initial fabric is completely modified by the deformation imposed upon the specimen.

2.2. Experimental procedure

The testing machine is heated externally and uses water as confining medium. For that reason, both the pressure vessel and the forcing pistons are made with Nimonic 105® alloy, a nickel-based alloy (75% nickel and 25% molybdenum) that is mechanically strong to temperatures in excess of 700 °C. During our experiments, the rock was tested dry with the pores vented to atmosphere. More detailed specifications of the testing machine can be found in Walker et al. (1990) and Covey-Crump (1992).

To be able to track strain changes by CPO patterns, we have performed the experiments at conditions well within the field of intracrystalline plasticity for calcite in Solnhofen limestone. These conditions are: 600 °C, a confining pressure of 200 MPa and a constant displacement rate of 5.2×10^{-6} m s^{-1}, the latter implying strain rates varying between initial 4.6 and finial 7.7×10^{-4} s^{-1}. Schmid et al. (1977) predicted that Solnhofen limestone at these strain rates would deform in the transition between the exponential and power law creep regimes (their regimes 1 and 2, see their fig. 2), well within the dislocation creep regime (see also their fig. 14). Despite the heterogeneous distribution of stress and strain rates, we have not seen in the microstructure effects of the operation of grain size sensitive flow mechanisms and we infer that the local differences in strain rates were not high enough to activate these mechanisms.

Cylinders of Solnhofen limestone 4 mm long and 9.5 mm in diameter were cored perpendicular to the bedding and placed in the pressure vessel between two spacers of 7% porosity Tennessee sandstone (7–8 mm long) (Fig. 3a). The Tennessee sandstone spacers were used to separate the pistons from the limestone specimen in order to vent the specimen pores to atmosphere without risk of sample extrusion into the hollow upper loading piston and to form a composite specimen assembly that could be thin-sectioned after the experiment without damage to the top and bottom surfaces of the limestone. Tennessee sandstone was selected because, whilst still being porous, it is much stronger than the limestone and therefore all deformation would occur within the limestone cylinder.

The limestone, sandstone and upper and lower spacers of Nimonic 105® alloy (2 mm thick), previously oven-dried at 80 °C, were placed inside an annealed copper jacket and then sealed with Nimonic 105® alloy rings (Fig. 3). The jacket isolated the specimen from the confining pressure medium. Due to the circumferential stretching of the cylinder, an extra-thick Cu jacket was used in some of the experiments (e.g. sf04) to avoid tearing of the jacket at high strains.

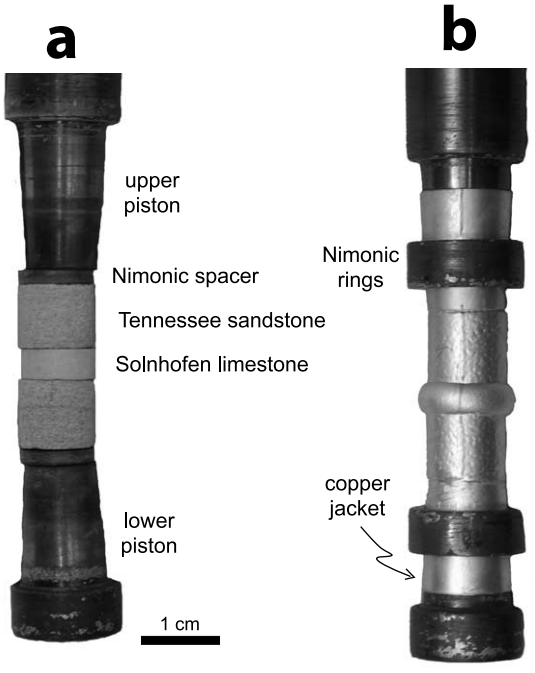

Fig. 3. Photographs of the specimen assembly in the experiments: before (a) and after (b) deformation.

2.3. Microstructural analysis

Two different sections of each deformed specimens were studied: parallel to and containing the axis of symmetry of the cylinder (named profile section); and parallel to the base of the cylinder. Most observations were done on profile sections. Deformed specimens were cut parallel to the profile and prepared as polished blocks to a surface finish of 0.05 μm gamma-alumina. EBSD analysis required further syton-polishing, but the occasional plucking out of quartz particles from the Tennessee sandstone that eventually scratch the limestone did not allow much improvement in the polish.

Owing to the high birefringence of calcite, it is possible

to observe the grains under reflected light in a conventional optical microscope. This was used for the micrographs in Figs. 7–9 after enhancing the brightness and contrast of the initial grayscale images (following Bestmann et al., 2000). Analysis of the crystallographic preferred orientation of calcite in the scanning electron microscope was done with the polished surfaces uncoated in the small maps in Fig. 10 and only required a very thin carbon coating for the overnight beam-scan runs that appear in Figs. 11 and 12. The CPO results are presented as pole figures of the major crystallographic axes and planes, i.e. *c*- and *a*-axes and poles to *r* planes, and also as inverse pole figures (IPF) using three orthogonal directions (nominally parallel to the radius, parallel to the bulk shortening axis, and normal to the other two, i.e. tangent to the cylinder everywhere but in the center). The first two directions were adjusted locally so they followed the orientation of the shape fabric where it became inclined to the basal plane of the cylinder. The first axis, which would otherwise be parallel to the radius, actually was the radial direction contained in an oblique foliation, and the second axis was chosen as the pole of this oblique foliation (Fig. 6).

3. Mechanical effects of axi-symmetric compression on short cylindrical specimens

In shortening experiments, the compressive force acting at right angles to the contact surface with the spacer/pistons imposes a non-slip condition along this surface. This has implications for the stress and strain distributions within the deformed specimen, as well as the bulk strength. As the specimen is made shorter, the frictional forces along those contacts oppose the outward spread of the specimen (see sketch in Fig. 1b). This produces the barreled shape in profile sections (Figs. 1b and 2b) and two conical regions of undeformed material extending from both pistons (Jaeger and Cook, 1976; Dieter, 1988).

In tests using long cylinders (referring to the length being greater than the diameter) the friction effects on overall specimen behavior are relatively small because the volume fraction affected by them is comparatively small. Thus, deformation throughout the specimens is relatively homogeneous and specimen strength approaches that representative of the material in bulk (Jaeger and Cook, 1976).

In short cylinders, however, when the length is smaller than the diameter (less than half in our experiments), the sample surface fraction affected by end-friction is much greater (Fig. 1). This increases the strength of the specimen well above that characteristic of the bulk material (Jaeger and Cook, 1976; Dieter, 1988). This effect is readily seen in our experimental results (Fig. 4). Also, in compressive tests on short cylinders, stresses and finite strain are expected to be heterogeneous. Strain rates are not constant during the experiments, neither globally nor locally. Jaeger (1962) presented the theoretical solution in 2D to the problem of radial channel flow between parallel plates approaching at constant speed for a linear viscous material. For such a type of material, he estimated that the force needed to deform the specimen had an inverse power law dependence on the radius/length ratio of the specimen as the pistons approached at constant speed (pp. 140–142 in Jaeger, 1962). For a non-linear material, as would be the case in Solnhofen limestone, a resistance to flow is similarly expected to increase as the specimen thickness decreases and strain rate increases.

When comparing mechanical data in experiments run

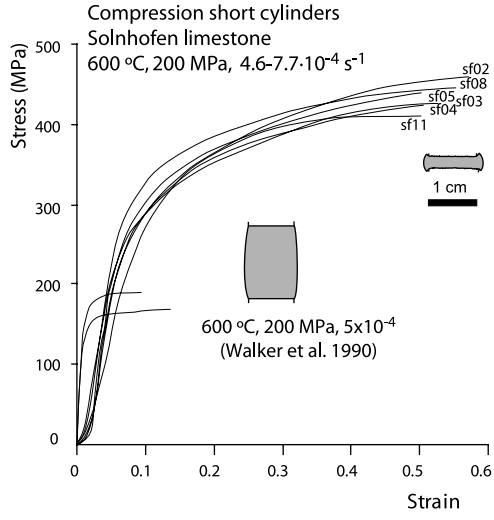

Fig. 4. Differential stress–strain curves obtained from the tests, illustrating first the reproducibility of the experiments with short cylinders and second the effect on strength of tests run on short cylinders in comparison with tests run on longer specimens. Mechanical data from long cylinders at similar strain rates, temperature and confining pressure in the same material are taken from fig. 4 in Walker et al. (1990). The curves in short cylinders have not been corrected for the strength of the copper jacket, which is estimated to be ca. 4 MPa.

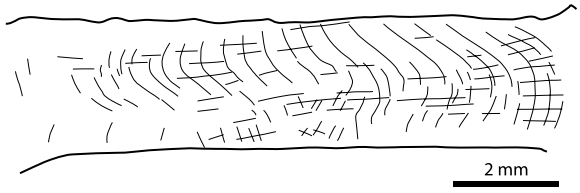

Fig. 5. Deformation of a Ni-grid and Au foil introduced prior to deformation in the middle of a split specimen (polished surfaces of the specimen parallel to the profile plane) after 40% permanent shortening (sample sf05). An initial irregularity in the Ni-grid produced an instability that ended with folding of the embedded metal layer in the middle and lower parts of the sample. However, the effect of the heterogeneous radial extrusion of the sample is still recorded in the shape of the initially rectangular grid. Note how the effects of the frictional forces at the contacts with the sandstone end pieces allows the development of the 'non-coaxial' component near the loading spacers (the vorticity axes in both upper and lower halves of the profile section are circumferential, therefore normal to the plane of the paper).

under similar constant displacement rates in short specimens (~4 mm long) with long ones (~20 mm long), one has also to take into account that the strain rates are initially five times faster in short specimens (corresponding to initially five times shorter specimens). The effect of strain rate on the strength of the specimen will also affect the mechanical behavior during the tests. In short samples, strain rates increase faster with progressive shortening than in long ones, hardening further the specimens (see the difference in slopes in stress–strain curves in Fig. 4 between the tests of Walker et al. (1990) and ours).

In an attempt to illustrate the strain distribution along the specimen profile, a test was performed using a split cylinder, where two orthogonal nickel grids were placed between the two polished specimen halves and separated by a central thin gold foil (as in Spiers, 1979). The high strains imposed on the specimen produced buckling of the nickel grids, which therefore clearly did not behave passively. Observations of the deformed grid (Fig. 5) were hindered by the degree of folding. However, they do illustrate the effect of the non-slip condition along the contact with the sandstone and the relative shear component of the flow as the middle part of the specimen was extruded. This allowed a rough estimate of the orientation of the principal finite strain directions throughout the specimen by observing how the initially orthogonal grid was deformed. This pattern was also followed by the orientation of the shape fabric (seen in Fig. 6). This is important because changes at local scale in the orientation and magnitude of principal stress directions will determine which slip systems operate according to their orientation. The geometry in Fig. 5 resembles the 'cream cake' strain effect in two dimensions (p. 613 in Ramsay and Huber, 1987), the difference being the switch in the extension direction from radial to circumferential (in and out of the paper) at the periphery of the rock cylinder.

4. Experimental results: microstructures

4.1. Shape and crystallographic fabrics

The finite shape fabric in calcite grains that developed after 50% shortening of specimen sf04, shown in Fig. 6, was traced by hand in the profile section from a collage of about 100 micrographs. The shape fabric map shows a few areas with distinctive patterns. The first type that we distinguish is in the middle of the specimen where flattening occurred continuously throughout the test. Grains are flattened and oriented parallel to the specimen base, defining an intense foliation (Fig. 7a). Provided the grains behaved as true strain markers, they should have an oblate shape in three dimensions. Note that despite the relatively high stresses (Fig. 5), they were still insufficient to produce twinning of the calcite grains.

The CPO patterns are symmetric in the pole figures (Fig. 10), similar to previous results under comparable experimental conditions (e.g. Kern, 1977, 1979). They are characterized by a *c*-axis great circle girdle within the foliation plane and a small circle girdle at about 40° from the pole of the shape fabric. In the inverse pole figure (IPF) along the shortening axis in Fig. 10, this is the $e+a/h$ type of fabric that is characteristic of calcite rocks shortened axisymmetrically at medium-high temperature (Spiers, 1979; Rutter et al., 1994).

The second distinctive area occurs near the contacts with the sandstone end pieces where an oblique shape fabric developed, dipping away from the axis of the cylinder (Fig. 7b and c). This fabric is curved and becomes parallel to the base of the sample near the outer confines of the pistons (Fig. 6). Only in the latter area is it possible to observe, in a section cut perpendicular to the sample axis, elongated grains oriented along the radial direction (Fig. 8a). *c*-Axis

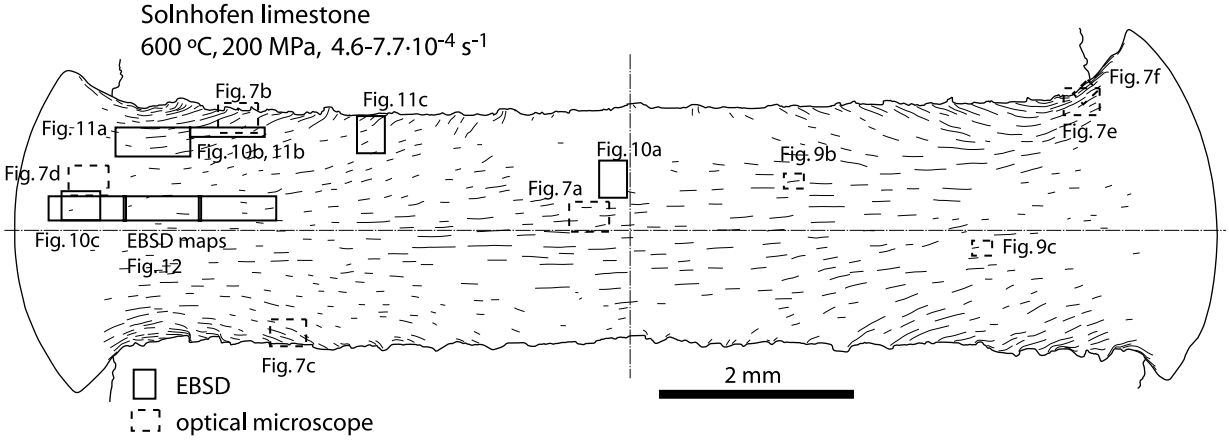

Fig. 6. Shape preferred orientation (SPO) map of calcite grains from the profile section of specimen sf04 drawn by hand. The location of the micrographs from Figs. 7–9, and the areas where CPO was measured using EBSD techniques, are also indicated by the boxes (dashed and black solid lines, respectively). The density and length of the traces indicate the relative strength of the shape fabric. Due to the large number of micrographs used to build this map there is a slight distortion in the direction parallel to the diameter of about +6% (the initial map was corrected with respect to the width). The ragged ends at the upper and lower surfaces of the specimen are the contacts with the Tennessee sandstone, where limestone was intruded into pore spaces in the sandstone.

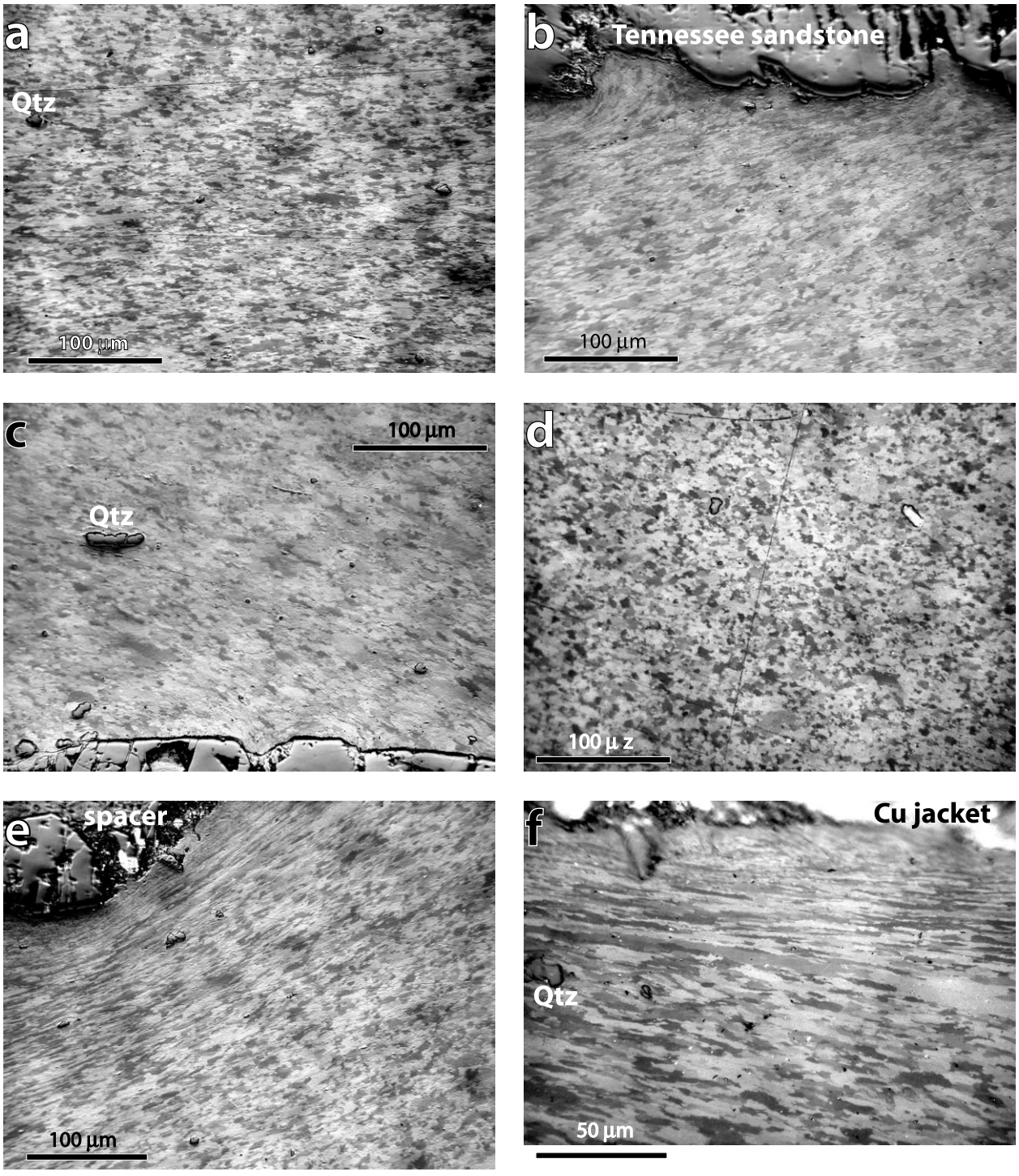

Fig. 7. Microphotographs taken under reflected light in an optical microscope from polished blocks showing the shape fabric developed in calcite grains in different key locations of the deformed specimens. The images were taken in the profile plane (parallel to the compression and sample axis), in: (a) the middle of the sample (flattening strain field, sample sf04); (b) and (c) near the contact with the sandstone, where an oblique foliation developed (general shear, sample sf04); (d) at the outer edge of the middle ring (field of circumferential extension, sample sf04); and (e) near one of the edges of the piston in specimen sf04 where sample deformation was concentrated. A detail of the latter is shown in (f).

pole figures show an internal asymmetry in the girdles that is consistent with the locally dextral sense of shear inherent to the development of the oblique fabric. In the IPFs, the local structural frame has been used (Fig. 10b). The pole of the shape fabric, regarded as the local shortening direction, is now at 22° from the bulk shortening axis (or Y_0). The direction corresponding to the local extension follows the radius, but it is contained within the foliation plane (22°

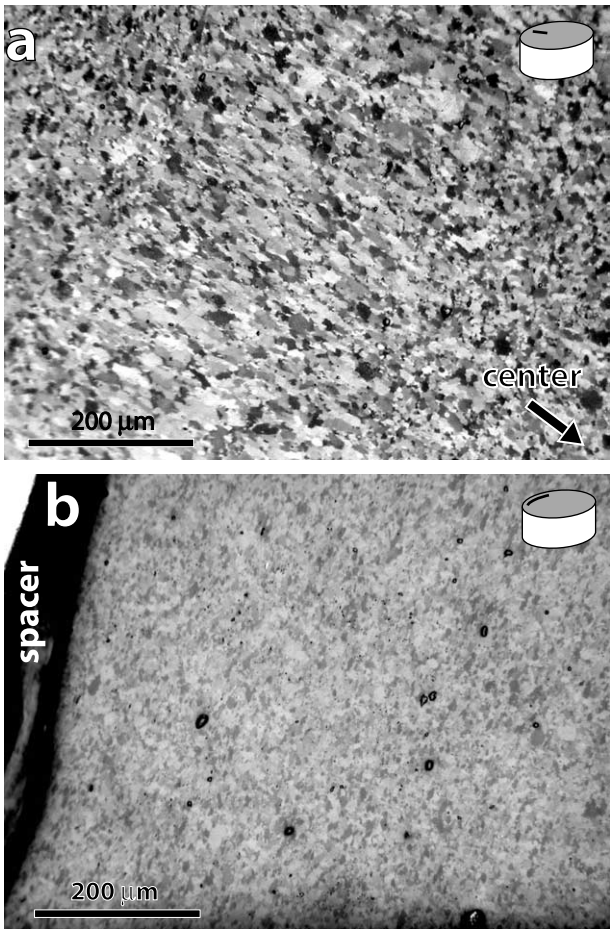

Fig. 8. Shape preferred orientation of calcite grains as seen under reflected light in a polished section (at an equivalent distance from the base of the sandstone spacer in sample sf04 of ca. 170 μm), but perpendicular to the compression axis (i.e. parallel to the base of the cylinder, as shown in the sketch). Micrograph in (a) is taken close to the corner of the sandstone spacer but still within the confines of the loading piston, and shows the radially-oriented extension in calcite grains where the foliation became parallel to the base of the cylinder. The micrograph in (b), close to the edge of the cylinder, illustrates the stretching of calcite grains following the circumference. Note from Fig. 6 that the shape fabric in calcite grains in the region close to a sandstone end piece (labeled 'spacer') is generally oblique and it only becomes parallel to the base of the cylinder in the vicinity of the confines of the pistons, close to the edges of the sandstone. The sketches in the photographs show in which surfaces the micrographs were taken.

from external X_0). Finally, the third direction corresponds to the vorticity axis of the local non-coaxial component involved, which is always circumferential due to the cylindrical symmetry (Z_0). An $e+a/h$ fabric is observed with respect to the pole to the shape fabric (Y_1).

The third characteristic area lies beyond the confines of the pistons, where stretching is everywhere parallel to the circumference of the cylinder. In sections cut parallel to the base, the elongation of calcite grains follows the specimen circumference (Fig. 8b) whereas in sections cut parallel to the profile, the grains remain equidimensional and an apparent decrease in grain size becomes recognizable, a geometric effect of the non-plane deformation in the plane of observation (Fig. 7d). Pole figures for the *c*- and *a*-axes show small circle girdles centered on the Z_0 direction (Fig. 10). The IPF with respect to the shortening axis was still parallel to the same external reference, Y_0, but stretching became aligned predominantly with Z_0. Pole figures are more familiar and thus easier to 'read' when presented in the tangential plane because the maximum stretching is then oriented E–W as is standard in structural geology (e.g. fig. 1 in Llana-Funez, 2002). The small circle girdle defined by the *c*-axes is in fact a double crossed girdle (Fig. 12).

4.2. Grain scale microstructures

In general, grain boundaries are straight and there is only limited evidence that any recrystallization has occurred. The microstructure is rather uniform locally and changes in grain shapes in response to changes in local principal strain directions are therefore expected to be an effect of intracrystalline plasticity as the predominant deformation mechanism. However, there is one major exception. It is in

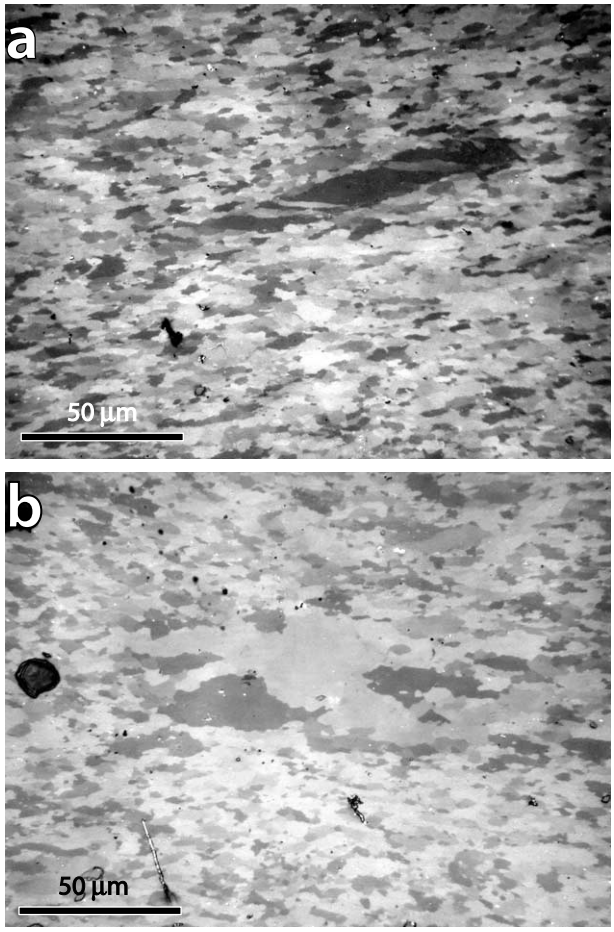

Fig. 9. Microstructures in calcite grains with an initially larger grain size than the 'matrix' (of about one order of magnitude larger). Twinning occurs in large grains located in the middle of the limestone specimen in (a). The twin boundaries are slightly bulged, probably indicating some boundary migration. Subgrains and lobate grain boundaries in (b) may be indicative of grain boundary migration in some of these large calcite grains.

the vicinity of the contact edges between the specimen and the Tennessee sandstone end pieces (Fig. 7e and f), where grain boundaries of extremely stretched grains are no longer straight but have developed a serrated profile and some small new grains are found. In the profile section there are four of these areas, which correspond to the intersection of two conical shear zones around the pistons, converging and overlapping towards the center of the specimen (see Figs. 1 and 6). These high-strain zones accommodate a rather large displacement in a relatively thin band. This implies not only high shear strains but also higher strain rates than anywhere else in the specimen. In consequence, the higher strain rate and hence flow stress may have promoted other processes to operate, such as twinning or rotation recrystallization.

It should be noted that the initially large (>40 μm) calcite grains that are occasionally found scattered in Solnhofen limestone, behaved in a different way to the finer grained and more uniform 'matrix'. They show grain size reduction, with the formation of subgrain structures, and also show evidence of twinning (Fig. 9a). Subgrain boundaries are no longer straight but become lobate (Fig. 9a and b). Some of the twins show slightly bulged boundaries (Fig. 9a). The initial grain size in these large grains was an order of magnitude larger than the average of the rock before the test and therefore it seems reasonable to expect that other processes may have been involved in their deformation.

4.3. Transition between areas with distinct strain types

To illustrate the progressive change in microstructure from an area with one strain geometry to another we present two traverses of EBSD maps crossing the edges of the loading spacers at two different levels. The first profile is close to one of the Tennessee sandstone end pieces, in order to include the region with the largest variation in orientation

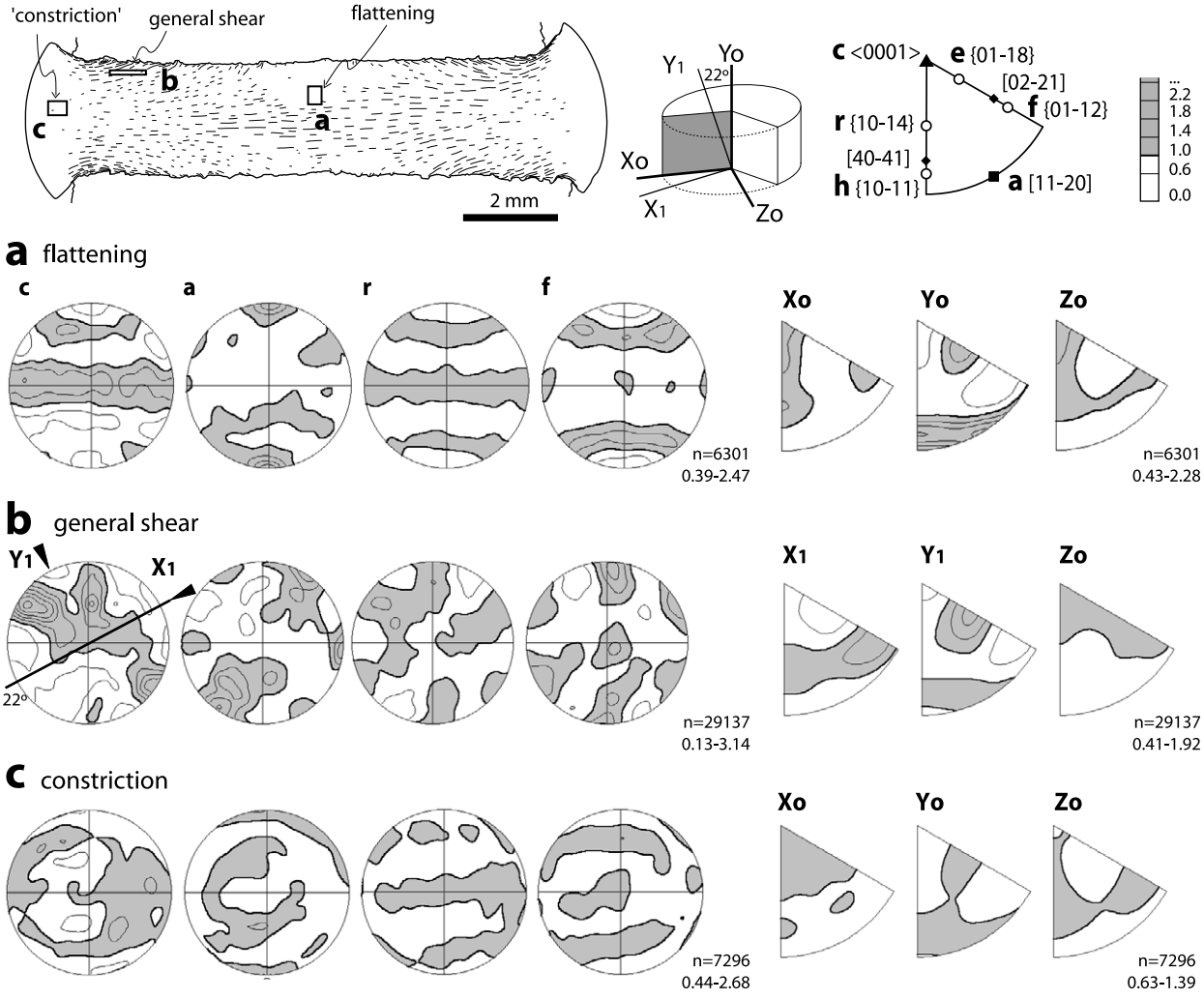

Fig. 10. Calcite CPO patterns measured in areas with distinct finite strain geometries: (a) near the middle of the specimen where flattening is predominant; (b) in the vicinity of the sandstone, where strain geometry is of general shear type; and (c) in the outer part of the cylinder, beyond the confines of the spacers/pistons, where strain approaches a constrictional geometry. In the upper left of the figure are located the EBSD study areas in the specimen profile. Legend in CPO figures is the same as is Fig. 2: contours are in 0.4 m.u.d. steps, starting at 0.6 and with shading above 1 m.u.d.

of the shape fabric (Fig. 11). EBSD maps in Fig. 10 are not all in contiguity, but they cross horizontally the trace of the oblique shape fabric starting at one of the ends of the deformed specimen (see location of maps in Fig. 6). The second profile runs along the middle of the specimen and records the initiation of circumferential stretching, starting in a region of predominantly flattening strain (Fig. 12).

The first set of maps (Fig. 11) registers a significant dextral non-coaxial deformation component. In *c*-axis pole figures, the single girdle parallel to the foliation initially seen in flattening strain areas becomes progressively less important and is restricted to a segment close to the intermediate axis, Z_0 in the external reference frame (Fig. 11c). On the other hand, the small girdle at 40° from the compression axis, characteristic of axi-symmetric flattening strain, becomes stronger and very asymmetric. In both textural components there is an internal asymmetry consistent with a dextral sense of shear for calcite. Overall, the pattern resembles a broad crossed girdle at right angles to the foliation, although we learn from the patterns in the neighboring area (area a in Fig. 10), dominated by axi-symmetric flattening strain, that it is made from two distinct and separate components, the single great circle girdle and the small circle girdle.

The second EBSD traverse was made along the equator of the specimen (Fig. 12), beginning in the middle of the specimen and progressing radially towards the outside. In the center, CPO patterns are characterized by a single *c*-axis great circle girdle sub-parallel to the foliation and a small circle girdle at 30–40° from Y_0. In contrast to the previous traverse, there is a significant external asymmetry in the innermost part of the studied area as both the single and small circle girdles are oriented at an angle to the shape fabric (in this area the foliation is parallel to the specimen base). This external asymmetry and the internal one defined in the small circle girdles, disappear towards the edges of the end pieces. At the same time, there is a progressive development of small circle girdles centered on the tangential axis (Z_0). Projected in a section parallel to the tangent of the cylinder (Fig. 12, below), the pattern would be of double crossed girdles resembling those predicted for quartz *c*-axes in constrictional deformation (Schmid and Casey, 1986). In our deformed specimens, the single *c*-axis girdle parallel to the foliation remains, yet the flattening

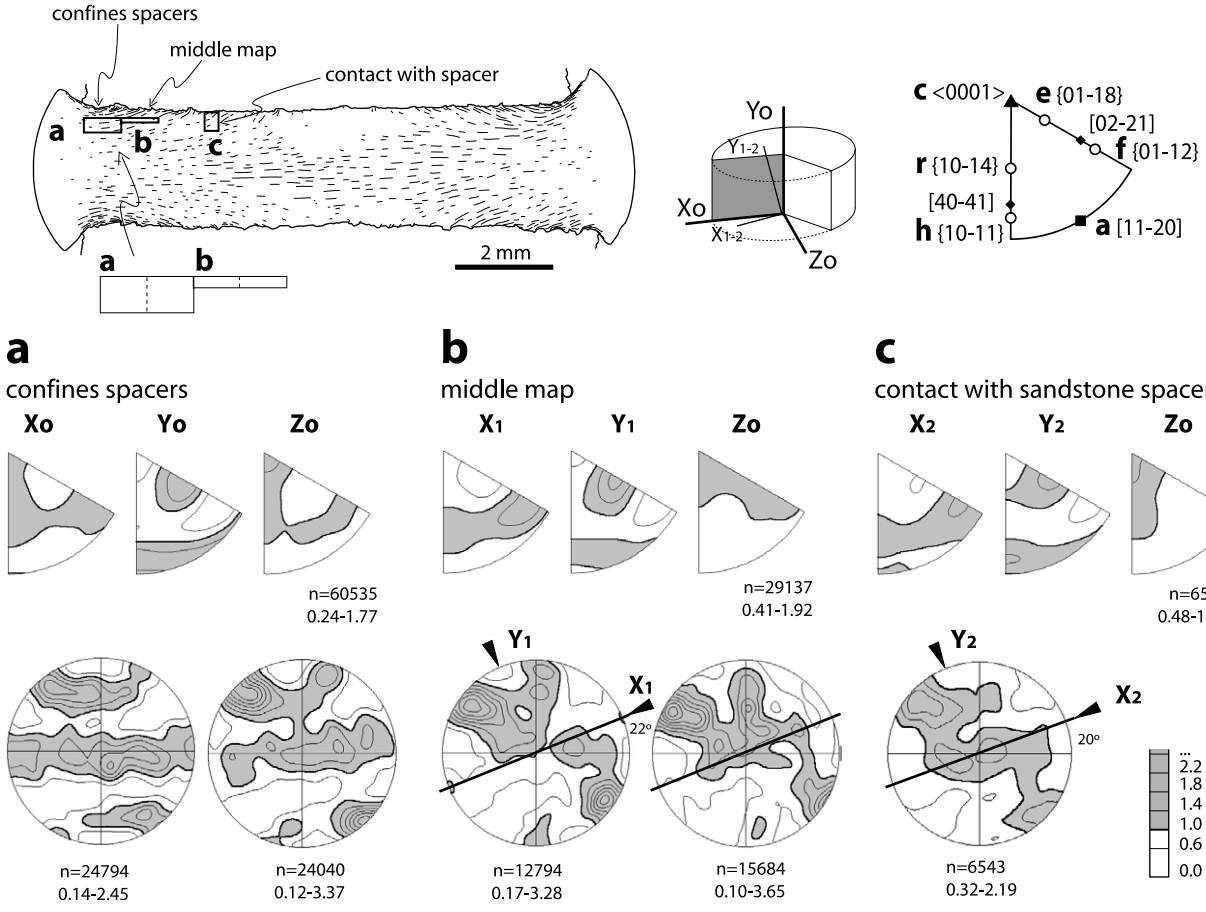

Fig. 11. Transect across the confines of the pistons close to one of the sandstone end pieces, illustrated by means of a combination of EBSD maps. The CPO patterns change progressively from being relatively asymmetric in the domain with oblique SPO to rather symmetric in the high strain area close to the edge of the specimen. Legends in IPF and pole figures are the same as in Figs. 2 and 10.

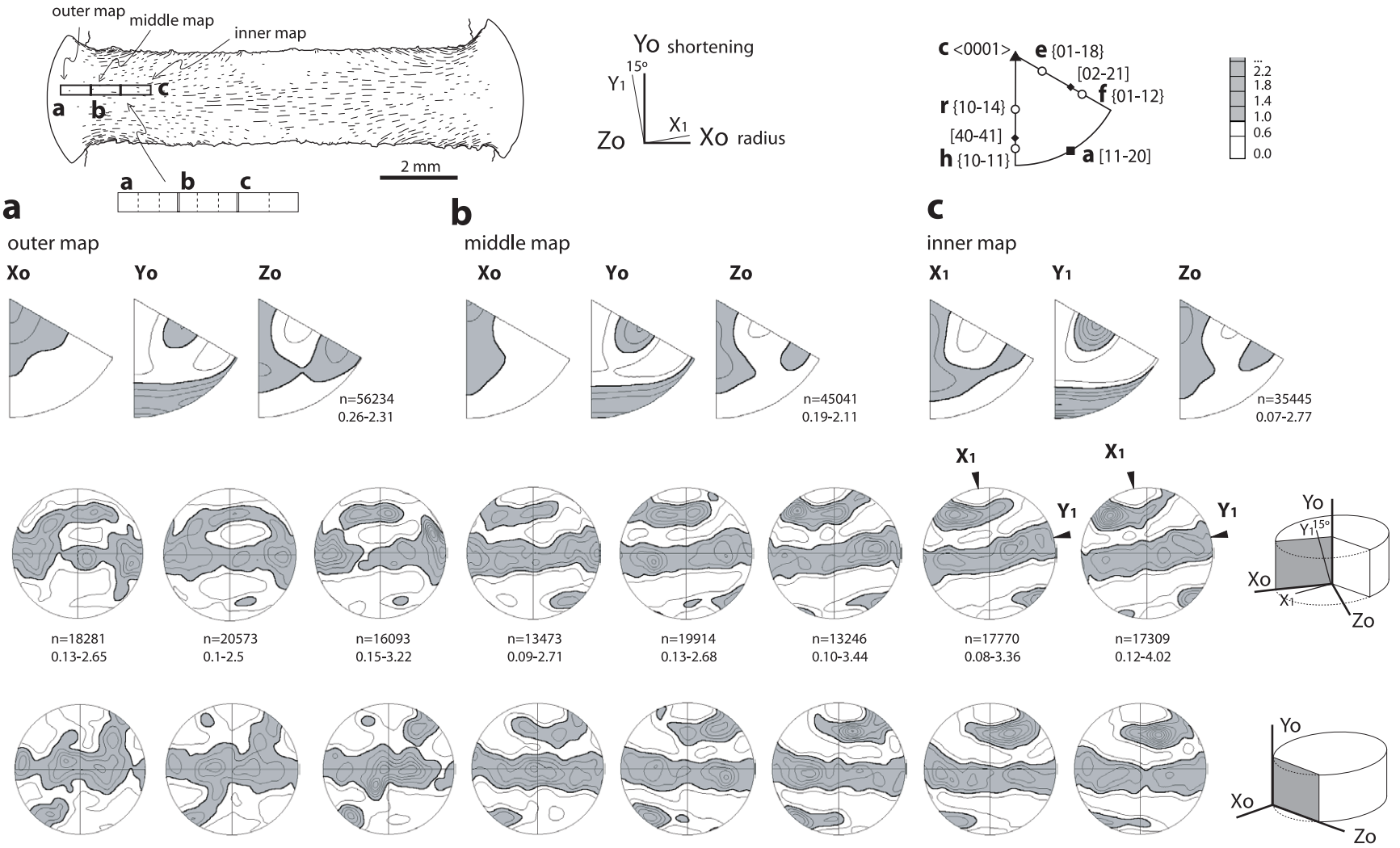

Fig. 12. Transect across the confines of the pistons at the 'equatorial' plane of the cylinder using EBSD maps. The IPFs record the change in extension direction from being along X_{0-1}, in the middle of the specimen, to Z_0 in the outside. It is also recorded neatly in the skeleton of the *c*-axis pole figures (further details in the text). Legends in IPF and pole figures are the same as in Figs. 2, 10 and 11.

component is predominant throughout the experiments. The IPFs in Fig. 12 show a strengthening of the extensional-type of pattern along the Z_0 direction, which is consistent with our observations on calcite grain shapes.

5. Discussion: use of CPO in rocks deformed under non-plane strain conditions

Axi-symmetric compression on short cylinders of Solnhofen limestone in experimental conditions favoring intracrystalline plasticity, provides ductilely deformed specimens with a varied range of non-plane strain geometries. This is so because the boundary conditions in the experiments impose very heterogeneous deformation in terms of strain geometry, as well as intensity. The results of our experiments show that the microstructures are reproducible. Qualitatively, the grain shapes seem to reflect strain geometry and are consistent with the CPO patterns. Individual deformed specimens are dominated by axi-symmetric flattening, but there are significant departures at local scale from axi-symmetric fabrics. The progressive change in, for instance, *c*-axis pole figure patterns from an area with one strain geometry to another also indicates that the aggregate keeps resetting efficiently according to the latest increment of strain, whether related to orientation of principal axes or their nature and relative magnitudes. The reorientation of the local principal strain directions determines the operation of those slip systems that are favorably oriented, in such a way that the combination of operative slip systems would accommodate the imposed local strain increments.

In calcite aggregates deformed plastically, distinct IPF fabrics are produced in shortening experiments ($e+a/h$ fabric) and in extension experiments (f or $f+(40\bar{4}1)$ fabric; see Fig. 10) (Wenk et al., 1986; Rutter et al., 1994). Here, we find simultaneously both patterns in the same measured areas because the first direction, X_0, represents the extension direction and the second, Y_0, the compressive direction. Specification of these two directions would be sufficient to describe the microstructure in rocks deformed in plane strain. In 3D deformation, a third direction has to be considered. If volume remains constant, this third direction will be either a second direction of shortening in constriction-dominated strains or a second direction of extension in flattening-dominated strains. We suggest that using the IPF for the third direction will help in discriminating whether it shortens or stretches and therefore allow us to differentiate between dominantly constrictional and flattening strains, although this concept has not been tested yet for naturally deformed rocks.

Although the types of CPO patterns in calcite rocks produced experimentally at medium-high temperature have not been reported from natural examples (Rutter et al., 1994), the principle of using IPFs in three orthogonal directions, including the principal shortening and extension directions, may prove of use when trying to estimate strain geometry in rocks deformed by non-plane strain. Alternatively, one could use the IPF patterns to infer the orientation of the maximum stretching when this direction is not clearly defined in a rock, for example when a pervasive recrystallization has obliterated the microstructure (provided it does not destroy the previous CPO) or if the rock does not present a well-defined lineation.

6. Conclusions

We have analyzed axi-symmetric shortening experiments from a new perspective, taking account of the full strain geometry when short cylindrical samples are used. We have extracted from different areas of the deformed specimens information regarding non-plane and non-coaxial strain, by making use of the heterogeneity of deformation and how it is recorded in the microstructure. The ultimate aim is to improve interpretation of naturally deformed rock bodies. Not only can one use the microstructures of high strain zones with predominantly simple shear flow to infer the kinematics, but one can also extract useful kinematic information from other strain zones departing from plane strain conditions, whether they are concentrated in discrete shear zones or affect larger volumes of heterogeneously deformed rocks.

Acknowledgements

This study was funded by Marie Curie Fellowship contract No. HPMF-CT-2000-00778, under the V Framework Program of the European Commission. Experimental officer Rob Holloway provided invaluable help in running the experiments. The testing machine was calibrated and kept in perfect state by Betty Mariani. Ian Brough from the Material Sciences Centre at Manchester Material Sciences Centre is also thanked for his assistance with the EBSD techniques. Thorough and constructive reviews by Jan Tullis and Hans de Bresser led to significant improvements to the manuscript.

References

Bestmann, M., Kunze, K., Matthews, A., 2000. Evolution of a calcite marble shear zone complex on Thassos Island, Greece: microstructural and textural fabrics and their kinematic significance. Journal of Structural Geology 22 (11–12), 1789–1807.

Casey, M., Kunze, K., Olgaard, D.L., 1998. Texture of Solnhofen limestone deformed to high strains in torsion. Journal of Structural Geology 20 (2/3), 255–268.

Covey-Crump, S.J., 1992. Application of a state variable description of inelastic deformation to geological materials. PhD Thesis, University College, London.

Dieter, G.E., 1988. Mechanical Metallurgy. McGraw-Hill, London.

Gilotti, J.A., Hull, J.M., 1993. Kinematic stratification in the hinterland of the central Scandinavian Caledonides. Journal of Structural Geology 15 (3/5), 629–646.

Jaeger, J.C., 1962. Elasticity, Fracture and Flow. Methuen & Co. and Wiley, London and New York.

Jaeger, J.C., Cook, N.G.W., 1976. Fundamentals of Rock Mechanics. Science Paperbacks, Chapman and Hall, London.

Jones, R.R., Holdsworth, R.E., Bailey, W., 1997. Lateral extrusion in transpression zones: the importance of boundary conditions. Journal of Structural Geology 19 (9), 1201–1218.

Kern, H., 1977. Preferred orientation of experimentally deformed limestone marble, quartzite and rock salt at different temperatures and states of stress. Tectonophysics 39, 103–120.

Kern, H., 1979. Texture development in calcite and quartz rocks deformed at uniaxial and real triaxial states of strain. Bulletin Minéralogie 102, 290–300.

Llana-Fúnez, S., 2002. Quartz c-axis texture mapping of a Variscan regional foliation (Malpica-Tui Unit, NW Spain). Journal of Structural Geology 24, 1299–1312.

Passchier, C.W., 1997. The fabric attractor. Journal of Structural Geology 19 (1), 113–127.

Passchier, C.W., 1998. Monoclinic model shear zones. Journal of Structural Geology 20 (8), 1121–1137.

Passchier, C.W., den Brok, S.W.J., van Gool, J.A.M., Marker, M., Manatschal, G., 1997. A laterally constricted shear zone system; the Nordre Stromfjord steep belt, Nagssugtoqidian Orogen, W. Greenland. Terra Nova 9 (5–6), 199–202.

Prior, D.J., Boyle, A.P., Brenker, F., Cheadle, M.C., Day, A., Lopez, G., Peruzzo, L., Potts, G.J., Reddy, S., Spiess, R., 1999. The application of electron backscatter diffraction and orientation contrast imaging in the SEM to textural problems in rocks. American Mineralogist 84 (11/12), 1741–1759.

Ramsay, J.G., Huber, M.I., 1987. The Techniques of Modern Structural Geology, Folds and Fractures, vol. 2. Academic Press, London.

Rutter, E.H., 1972. The influence of interstitial water on the rheological behaviour of calcite rocks. Tectonophysics 14, 13–33.

Rutter, E.H., 1998. Use of extension testing to investigate the influence of finite strain on the rheological behaviour of marble. Journal of Structural Geology 20 (2/3), 243–254.

Rutter, E.H., Casey, M., Burlini, L., 1994. Preferred crystallographic orientation development during the plastic and superplastic flow of calcite rocks. Journal of Structural Geology 16 (10), 1431–1446.

Sander, B., 1950. Einführung in die Gefügekunde der Geologischen Körper. II: die Korngefüge. Springer, Wien.

Schmid, S.M., Casey, M., 1986. Complete fabric analysis of some commonly observed quartz *c*-axis patterns. In: Hobbs, B.E., Heard, H.C. (Eds.), The Paterson Volume American Geophysical Union Monographs, vol. 36, pp. 263–286.

Schmid, S.M., Boland, J.N., Paterson, M.S., 1977. Superplastic flow in finegrained limestone. Tectonophysics 43, 257–291.

Spiers, C., 1979. Fabric development in calcite polycrystals deformed at 400 °C. Bulletin Minéralogie 102, 282–289.

Walker, A.N., Rutter, E.H., Brodie, K.H., 1990. Experimental study of grain-size sensitive flow of synthetic, hot-pressed calcite rocks. In: Knipe, R.J., Rutter, E.H. (Eds.), Deformation Mechanisms, Rheology and Tectonics Geological Society Special Publication, vol. 54, pp. 259–284.

Wenk, H.R., Kern, H., van Houtte, P., Wagner, F., 1986. Heterogeneous strain in axial deformation of limestone, textural evidence. In: Hobbs, B.E., Heard, H.C. (Eds.), The Paterson Volume American Geophysical Union Monographs, vol. 36, pp. 287–295.